JOURNAL OF SOLID STATE CHEMISTRY 110, 66–69 (1994)

Tetrahedral Coordination of Mn(IV) by Oxygen in Manganese Sillenite $Bi_{12}MnO_{20}$

U. Delicat, S. F. Radaev, and M. Trömel[1]

Institut für Anorganische Chemie der J. W. Goethe-Universität, Marie Curie-Str. 11, D-60439 Frankfurt a. M. 50, Germany

P. Behrens

Fakultät für Chemie, Universität Konstanz, Universitätsstraße 10, D-78464 Konstanz 1, Germany

and

Y. F. Kargin and A. A. Mar'in

Institute of General and Inorganic Chemistry, Russian Academy of Sciences, Leninsky pr. 31, 117071 Moscow, Russia

Received June 8, 1993; accepted August 6, 1993

Polycrystalline samples and a single crystal of the Mn sillenite $Bi_{12}MnO_{20}$ have been synthesized and studied. IR spectroscopy, XANES, and XRPD show that manganese atoms are tetravalent and tetrahedrally coordinated by oxygen. The X-ray single-crystal study of $Bi_{12}MnO_{20}$ confirms that this is the first example of a compound containing Mn^{IV} in tetrahedral coordination by oxygen with Mn–O distances of 1.75(2) Å. The crystal is cubic, sp.gr. *I*23 ($Z = 2$); $a = 10.206(1)$ Å. The final agreement factors are $wR = 2.83$ and $R = 3.49\%$ for 625 reflections. $Bi_{12}MnO_{20}$ belongs to the stoichiometric sillenites with tetravalent *M* atoms of one kind. © 1994 Academic Press, Inc.

INTRODUCTION

The large structural family of bismutates with sillenite structure (1) is of interest due to some special physical properties such as photorefraction, piezoelectricity, and optical activity. Stoichiometric sillenites $Bi_{12}MO_{20}$ contain tetravalent atoms, e.g., Si, Ge, Ti, which occupy position (2*a*) in space group *I*23 with ideal tetrahedral coordination by oxygen. A Bi–O framework connects the MO_4 tetrahedra, in which Bi(III) with a stereochemically active lone pair is (5 + 2) coordinated (2). A large number of elements with oxidation states other than four can be incorporated in the (2*a*) position of sillenites, giving rise to nonstoichiometric sillenites. Charge balance then is achieved by oxygen vacancies, substoichiometry with regard to *M*, and concomitant partial occupation of the (2*a*) sites by Bi(III) or, in the case of *M* atoms with valence >IV, incorporation of additional oxygen in interstitial sites (3).

The most thoroughly studied sillenites are the stoichiometric compounds $Bi_{12}SiO_{20}$ (4), $Bi_{12}GeO_{20}$ (2), and $Bi_{12}TiO_{20}$ (3). Speer and Jansen (5) quoted the formula $Bi_{12}MnO_{20}$ for a manganese sillenite, which implies that the mean valence of manganese in this compound is 4. Mn(IV) seems to be unknown in tetrahedral coordination by oxygen. In quaternary sillenite compounds with *M* combinations of, e.g., (Li, Mn), (Zn, Mn), or (Fe, Mn), tetrahedrally coordinated manganese has been proven to be pentavalent (5, 6). Therefore, the structural details of the ternary manganese sillenite, the oxidation state of Mn, and its local environments in this compound are of general interest with regard to the coordination chemistry of transition metals in solid-state oxides.

EXPERIMENTAL

Polycrystalline samples of manganese sillenite were prepared by solid-state reactions of special-purity α-Bi_2O_3 (99.9%, Janssen) and MnO_2 (99.99%, Aldrich). Homogenized mixtures of the oxides (atomic ratio 12 Bi to 1 Mn) were heated in a gold crucible for 107 hr at 700°C with intermittent grinding in order to obtain pure phases. Sintered specimens were cooled to room temperature.

The dark-green powder was initially characterized by XRPD on a Rigaku Denki SG-9R using Ni-filtered Cu$K\alpha$ radiation showing the typical diffraction pattern of sillenites. The X-ray powder pattern of the pure phase will be submitted to International Centre for Diffraction Data, Newton Square, Pennsylvania, U.S.A., for the Powder

[1] To whom correspondence should be addressed.

0022-4596/94 $6.00

Data File. Reflection intensities were calculated with the program LAZY PULVERIX (7).

MnK edge spectra of Mn sillenite and of Mn–O reference compounds were measured at room temperature at the EXAFS II beamline at HASYLAB/DESY (Hamburg, Germany). Data were collected in transmission mode on pressed polyethylene pellets. For the sillenite, the Mn content was adjusted to give an edge jump of only $\Delta\mu d \approx 0.2$ in order to avoid too high background absorption from bismuth. Edge jumps of MnO, Mn_3O_4, and MnO_2 were $\Delta\mu d \approx 1.0$. Spectra were corrected for pre-edge background absorption and normalized. The IR absorption spectra were determined on CsI pellets using a Perkin–Elmer spectrometer 283B.

High purity Bi_2O_3 and $Mn(NO_3)_2 \cdot 6H_2O$ were used to prepare $Bi_{12}MnO_{20}$ single crystals by the hydrothermal method. The experiments were carried out at 250–300°C and pressures up to 1000 kg cm^{-3}. Aqueous solutions of 30 wt.% NaOH were used as solvent. Crystals were grown by spontaneous crystallization for 10–45 days. The small cubic crystals were very dark green, almost black.

Attempts to grind spheres were unsuccessful, because after grinding no diffraction pattern could be obtained. Therefore, a single crystal of distorted tetrahedral shape with faces (100), (010), (001), and ≈ (111) ($V = 1.84 \cdot 10^{-3}$ mm^3) was selected for the X-ray diffraction study. The diffraction data were collected on an Enraf–Nonius CAD-4 diffractometer at room temperature. The lattice constant $a = 10.206(1)$ Å was refined by least-squares from 25 reflections with $20 < \Theta < 24°$. A total of 5460 reflections was measured using Mo$K\alpha$ radiation (graphite monochromator, $\lambda = 0.71076$ Å), ω-scan mode, in a reciprocal hemisphere ($l \geq 0$) of radius $\sin\Theta/\lambda = 1.0$ $Å^{-1}$. The data were corrected for X-ray absorption using numerical integration with a 16 × 16 × 16 network, $\mu = 943.1$ cm^{-1}. Analysis of the systematic absences and a subsequent averaging of symmetry-equivalent reflections confirmed the space group $I23$. Errors caused by absorption prevented a reliable determination of the absolute configuration. Therefore, the data were averaged in point group $m3$. The $\Delta f''$ corrections were neglected in the calculation of structure factors. Finally, after Lorentz and polarization corrections 625 independent reflections with $I \geq 3\sigma(I)$ were used for the refinement of the structure. An isotropic extinction correction was applied: $g = 0.31 \cdot 10^{-4}$, Becker and Coppens formalism, type I, Lorentzian distribution (8). All calculations were carried out using the program PROMETHEUS (9). Scattering curves of neutral atoms and $\Delta f'$ corrections were taken from (10).

RESULTS

Chemical analysis. According to Devalette *et al.* (6), the presence of Mn^V can be tested by dissolving the Mn sillenite in 3 *N* nitric acid. By disproportionation the violet color of $[MnO_4]^-$ ions will appear. No pentavalent Mn was found, in agreement with (5). In addition, the Bi^V content in the Mn sillenite has been tested by a modified iodometric method (11). Within the limits of error no Bi^V was detected.

TABLE 1

Selected Relative X-ray Powder Reflection Intensities of Mn Sillenite $Bi_{12}MnO_{20}$ and Calculated Intensities for Sillenites $(Bi_{12})MnO_{20}$ and $(Bi_{11}Mn)BiO_{20}$

	110	200	220	222	411	420	332
Experimental	0.5	2.9	23.1	22.9	7.9	9.1	14.3
$(Bi_{12})MnO_{20}$	0.9	2.8	23.3	23.2	7.6	9.2	14.4
$(Bi_{11}Mn)BiO_{20}$	2.3	0.2	12.5	27.6	3.6	4.8	8.2

Note. Atoms in (24*f*) in parentheses.

X-ray powder diffraction. On the basis of the model for $Bi_{12}GeO_{20}$ (2) and the sample composition $Bi_{12}MnO_{20}$ we calculated the intensities for different distributions of Mn and Bi over the cation sites. Marked differences in the calculated intensities of the reflections 110, 200, 220, 222, 411, 420, and 332 are observed (Table 1). Comparison between calculated and observed intensities clearly shows that Mn atoms occupy the (2*a*) position.

IR absorption spectra. Mn sillenite has prominent absorption bands in the region of 400–600 cm^{-1}, corresponding to vibrations of the bismuth–oxygen framework, and a higher-frequency absorption at 715 cm^{-1} (Fig. 1). The latter was supposed to be an internal mode of the Mn–O tetrahedron. As known from Venugopalan and Ramdas (12, 13) and Betsch and White (14), the high-frequency part of the vibrational spectra of sillenites with Si, Ge, and Ti exhibits bands of tetrahedrally coordinated atoms. In Fig. 1, the ν_3 absorption bands of tetrahedral $[MnO_4]^{n-}$

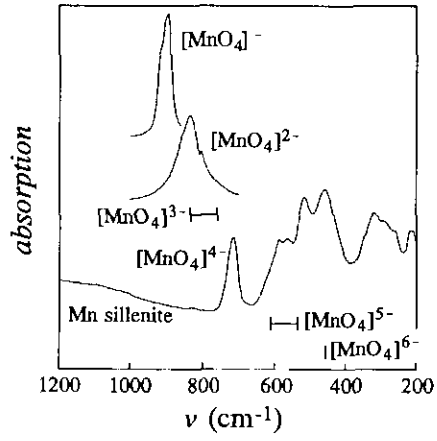

FIG. 1. Infrared spectra of polycrystalline powders of Mn–O compounds with tetrahedrally coordinated Mn.

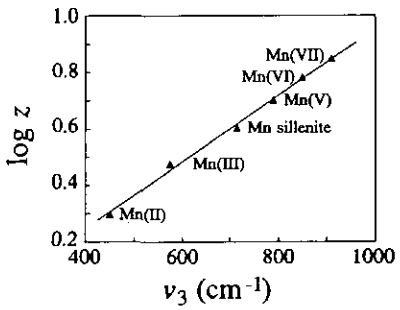

FIG. 2. Plot of logarithm of oxidation state z against wave numbers ν_3 of $[MnO_4]^{n-}$ groups.

groups of model compounds ($KMnO_4$, K_2MnO_4) and IR data reported by Preudhomme and Tarte (15), viz. $Ba_3(MnO_4)_2$, $Sr_2Mn_2GeO_7$, and $Sr_2MnSi_2O_7$ are shown. Obviously, the band at 715 cm^{-1} in the Mn sillenite spectrum corresponds to the asymmetric stretching mode ν_3 of tetrahedrally coordinated Mn (point symmetry T). Applying the empirical relation (11)

$$\log z = 1.158 \times 10^{-3}\, \nu_3\ (\mathrm{cm}^{-1}) - 0.211$$

(with ν_3 = vibration frequencies of tetrahedral $[MnO_4]^{n-}$ oxo anions) the oxidation state z of Mn in the sillenite was calculated as $4.1 \approx 4$ (Fig. 2).

XANES measurements at the MnK edge. We used MnK edge XANES spectra of Mn sillenite and of Mn–O compounds with known oxidation states and coordination geometries as fingerprints (16). K edge absorption spectra of first-row transition metal atoms exhibit one or several pre-edge peaks at energies slightly below the edge energy. These are caused by dipole-forbidden $1s \rightarrow 3d$ transitions of the excited electrons. The intensity of these pre-edge features depends on the local environments of the absorbing atom. Intensity differences allow a distinction between, e.g., tetrahedral and octahedral coordination geometry. The exact position of the pre-edge features and the edge position shift to higher energies with increasing oxidation state of the absorbing atom.

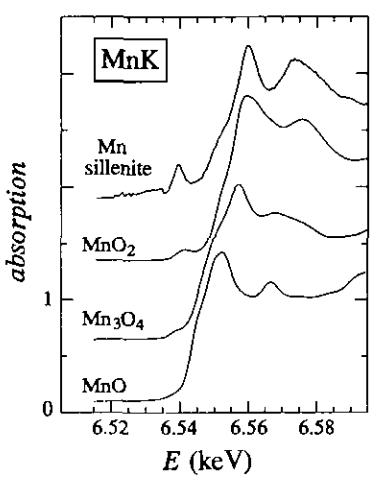

FIG. 3. MnK XANES spectra for a series of Mn–O compounds.

The XANES spectra shown in Fig. 3 exhibit corresponding high energy shifts on going from Mn(II) in MnO, Mn(II,III) in Mn_3O_4 to Mn(IV) in MnO_2. The features in Mn sillenite occur at positions similar to those observed for MnO_2, strongly indicating that the oxidation state is Mn(IV). Comparison with investigations in the literature rule out the presence of higher-valent Mn (17, 18). The pre-edge peak located at about 6.54 keV is much more intense for the sillenite than for MnO_2, where Mn(IV) is in octahedral coordination. This is in full agreement with a tetrahedral coordination (19, 20). The considerable width of the sillenite pre-edge peak as compared with corresponding signals in spectra of other tetrahedrally coordinated transition metal atoms seems to be typical of K edge spectra of M atoms in sillenites. This has also been observed for Ti and Fe sillenites (11). This indicates a broadening of the d states of the metal atoms; i.e., the d states cannot be regarded as local any more but are part of a band-like electronic structure. Our interpretation is that there is strong electronic interaction between the M atoms and the Bi–O framework.

Structure determination. Refinement of the standard structural model (2, 4) using anisotropic thermal parameters led to $wR = 2.83$ and $R \approx 3.49\%$[1]. The analysis of residual electron density maps did not reveal any deviations from the model (2, 4). The main task was to check the occupancy factor of the Mn position. Full matrix refinement and a subsequent checking of the occupancy factor by a step-by-step scanning technique (21) indicate that the minimum of R factors corresponds to $q_{Mn} = 1.00(6)$ and $B_{Mn} = 1.0(2)$ Å^2. As mentioned earlier (22), it is practically impossible to determine reliably the occupancy factors of oxygen atoms in sillenites by X-ray diffraction due to the small scattering power of oxygen atoms and a strong correlation between occupancy q and the thermal parameter B. Therefore, the occupancy factors of oxygen were not refined. The structural parameters of the model are listed in Table 2, the main interatomic distances and angles in Table 3.

DISCUSSION

Our results confirm the formula $Bi_{12}MnO_{20}$ of manganese sillenite as a stoichiometric compound. Tetravalent manganese only occupies the tetrahedrally coordinated

[1] $wR = \sqrt{\dfrac{\Sigma_w(|F_{obs}| - |F_{calc}|)^2}{\Sigma_w F_{obs}^2}}$; $w = [\sigma(F_{obs})]^{-2}$; $R = \dfrac{\Sigma||F_{obs}| - |F_{calc}||}{\Sigma|F_{obs}|}$.

TABLE 2
Fractional Atomic Coordinates and Equivalent Isotropic Thermal Parameters (Å^2) with e.s.d.s in Parentheses

	x	y	z	B_{eq}
Bi	0.17771(5)	0.32109(5)	0.02207(5)	1.039(7)
Mn	0	0	0	1.0(2)
O(1)	0.1345(8)	0.2478(8)	0.4902(8)	1.1(1)
O(2)	0.2015(10)	0.2015(10)	0.2015(10)	1.8(3)
O(3)	0.901(1)	0.901(1)	0.901(1)	2.8(5)

Note. $B_{eq} = (4/3)\Sigma_i \Sigma_j \beta_{ij}\mathbf{a}_i\mathbf{a}_j$.

sites (2*a*). $Bi_{12}MnO_{20}$ is the first example of Mn(IV) in tetrahedral coordination by oxygen. Similar to other ions with a $3d^3$ configuration, e.g. Cr^{3+}, Mn^{4+} strongly prefers octahedral coordination (compare (23)). The stabilization of the unusual tetrahedral coordination of Mn(IV) in Mn sillenite is in line with the observation that many elements with oxidation states ranging from +I to +VI (possibly in Cr sillenite) can be incorporated on the (2*a*) site of the sillenite structure, disregarding their different chemical properties and coordination demands.

As in other cases our result is in good agreement with the bond length of Mn–O bonds as predicted by Trömel (24) ten years ago:

		predicted (Å)	experimental (Å)	literature
Mn_2O_7,	bridge	1.76	1.762(3)	(25)
	terminal	1.58	1.575(3), 2 × 1.588(3)	(25)
Mn(V),	tetrahedral	1.69	1.70(1)	(26)
Mn(IV),	tetrahedral	1.76	1.75(2)	this work

TABLE 3
Main Interatomic Distances (Å) and Angles (°) with e.s.d.s in Parentheses

Bi–O(1*a*)	2.067(8)	O(1*a*)–Bi–O(1*b*)	92.7(1)
Bi–O(1*b*)	2.193(8)	O(1*a*)–Bi–O(1*c*)	84.3(1)
Bi–O(1*c*)	2.603(8)	O(1*a*)–Bi–O(2)	80.9(3)
Bi–O(1*d*)	3.064(8)	O(1*a*)–Bi–O(3*f*)	85.4(3)
Bi–O(1*e*)	3.314(8)	O(1*b*)–Bi–O(1*c*)	69.5(3)
Bi–O(2)	2.214(4)	O(1*b*)–Bi–O(2)	88.0(5)
Bi–O(3*f*)	2.706(8)	O(1*b*)–Bi–O(3*f*)	174.9(3)
		O(1*c*)–Bi–O(2)	152.3(5)
		O(1*c*)–Bi–O(3*f*)	115.0(4)
		O(2)–Bi–O(3*f*)	87.0(5)
Mn–O(3)	4 × 1.745(21)		

Symmetry codes: (*a*) 1/2 − *x*, 1/2 − *y*, −1/2 + *z*; (*b*) *y*,*z*,*x*; (*c*) *y*, 1 − *z*, −*x*; (*d*) −1/2 + *z*, 1/2 + *x*, 1/2 − *y*; (*e*) 1/2 −*z*, 1/2 − *x*, −1/2 + *y*; (*f*) 1 − *x*, 1 − *y*, −1 + *z*.

Using the effective ionic radii (27) for Mn(IV) (r = 0.39 Å) and for O(II) (r = 1.38 Å) the Mn–O distance is calculated as 1.77 Å, which is also in good agreement with our results.

ACKNOWLEDGMENTS

The authors are indebted to the Deutsche Forschungsgemeinschaft for support of this study and the Hamburger Synchrotonstrahlungslabor (HASYLAB), Hamburg, Germany for allocating beam time. We are grateful to Dr. P. Kizler (DESY-HASYLAB, Hamburg, Germany) for his help in data collection. The present work has been financially supported by the Alexander von Humboldt-Stiftung to one of us (S.F.R.).

REFERENCES

1. E. M. Levin and R. S. Roth, *J. Res. Natl. Bur. Stand., Sect. A* **68,** 197 (1964).
2. S. C. Abrahams, P. B. Jamieson, and J. L. Bernstein, *J. Chem. Phys.* **47,** 4034 (1967).
3. S. F. Radaev, V. I. Simonov, Y. F. Kargin, and V. M. Skorikov, *Eur. J. Solid State Inorg. Chem.* **29,** 383 (1992).
4. S. C. Abrahams, J. L. Bernstein, and C. Svensson, *J. Chem. Phys.* **71,** 788 (1979).
5. D. Speer and M. Jansen, *Z. Anorg. Allg. Chem.* **542,** 153 (1986).
6. M. Devalette, N. Khachani, G. Meunier, and P. Hagenmuller, *Mater. Lett.* **4B,** 318 (1984).
7. K. Yvon, W. Jeitschko, and E. Parthé, *J. Appl. Cryst.* **10,** 73 (1977).
8. P. J. Becker and P. Coppens, *Acta Crystallogr., Sect. A* **30,** 148 (1974).
9. U. H. Zucker, E. Perenthaler, W. F. Kuhs, R. Bachman, and H. J. Schulz, *J. Appl. Cryst.* **16,** 358 (1983).
10. International Tables for X-Ray Crystallography, The Kynoch Press, Birmingham, 1974.
11. U. Delicat, Thesis, Frankfurt a. M. 1993.
12. S. Venugopalan and A. K. Ramdas, *Phys. Rev. B* **5,** 4065 (1972).
13. S. Venugopalan and A. K. Ramdas, *Phys. Rev. B* **8,** 717 (1973).
14. R. J. Betsch and W. B. White, *Spectrochim. Acta, Part A* **34,** 505 (1977).
15. J. Preudhomme and P. Tarte, *Spectrochim. Acta, Part A* **27,** 961 (1971).
16. P. Behrens, *TrAC, Trends Anal. Chem. (Pers. Ed.)* **11,** 237 (1992).
17. R. M. Nayak and B. D. Padalia, *Phys. Status Solidi B* **96,** 259 (1979).
18. G. B. Bunker, Thesis, Univ. of Washington, Seattle, 1984.
19. P. Behrens, U. Delicat, and M. Trömel, HASYLAB Jahresbericht 1992, p. 235, 1992.
20. P. Behrens, U. Delicat, and M. Trömel, *Z. Kristallogr. Suppl. Issue* **7,** 16 (1993).
21. L. A. Muradyan, S. F. Radaev, and V. I. Simonov, "Methods of Structural Analysis," p. 5. Nauka, Moscow, 1989.
22. S. F. Radaev, L. A. Muradyan, and V. I. Simonov, *Acta Crystallogr., Sect. B* **47,** 1 (1991).
23. D. M. Sherman, *Am. Mineral.* **69,** 788 (1984).
24. M. Trömel, *Acta Crystallogr., Sect. B* **39,** 664 (1983).
25. A. Simon, R. Dronskowski, B. Krebs, and B. Hettich, *Angew. Chem.* **99,** 160 (1987).
26. D. Reinen, H. Lachwa, and R. Allmann, *Z. Anorg. Allg. Chem.* **542,** 71 (1986).
27. R. D. Shannon, *Acta Crystallogr., Sect. A* **32,** 751 (1976).